Instructions for Book Chapter Proofs

Please read your proof carefully, our staff won't read it in detail after you have returned it.
Final responsibility for content lies with the author.

- Corrections should be marked on the **PDF proof using electronic notes**. Please do **not** send a revised Word file as we will not be able to use it.
- Correct only **errors**. Rewriting sections or making minor textual changes is not allowed at this stage.
- Please clearly respond to all the **author queries** listed on the following page. Put your responses **in the text** and not on the query page. Click on the query number to jump to the relevant place in the text.
- If **Figures** need correcting, please resupply a new file at the highest possible resolution.
- **Non-native English speakers**: we recommend asking a native English speaking colleague to proof read all content before sending the final corrections.

Please check:

- **Special characters** (e.g. Greek letters/dashes/superscripts) appear correctly. This is especially important in equations.
- **Figures** are correct (they will be printed in color as they appear in the proof).
- **Headings and sub-headings** are correctly placed.
- **Copyright acknowledgements** for images reproduced from another source are present and correct, and you have sent copies of the permission to the RSC.

Please note:

- This is a **web quality pdf**, a higher resolution file will be used for the print book.
- Corrections **must not affect the pagination**.

Please **e-mail an annotated PDF (electronic notes)** within **ONE WEEK** of receipt of your proof to: fm202@bath.ac.uk and david.fermin@bristol.ac.uk

If you have any queries, please do not hesitate to contact us at: booksprod@rsc.org

Books Production Team

AUTHOR QUERY FORM

Book Title: Electrochemical Reduction of Carbon Dioxide: Overcoming the Limitations of Photosynthesis
Chapter 6

Please indicate the changes required in response to the queries within the text. If no changes are needed please clearly state this next to the query marker.

AQ1	The equations appear to be labelled out of numerical order. Please check that the numbering is correct and indicate the changes required.
AQ2	Ref. 21: Please provide the title.
TS1	The running head has been shortened to fit the space available. Please check that the text is suitable.

Abstract

The abstract for your chapter is reproduced below for your reference. Please note that this will **not** appear in the final printed version of your chapter.

The computer-aided molecular modelling of the catalytic conversion of carbon dioxide (CO_2) into 'green' fuels offers a comprehensive view of the chemical events taking place during the process. This provides crucial information about 'where', 'how', and 'why' and also allows the *in silico* hypothesising of those promising catalysts before the experimental testing of their catalytic performance. Among the variety of quantum mechanical approaches, well-resolved density functional theory (DFT) has been proven as a fast, robust, and powerful methodology for such purposes. In the present chapter, we review different fundamental aspects of the chemical reactivity with special emphasis on the theoretical point-of-view as well as fully treating the thermodynamics, kinetics, and additional aspects for the DFT modelling of the CO_2 conversion mechanism screening through the electrochemical approach.

CHAPTER 6

DFT Modelling Tools in CO_2 Conversion: Reaction Mechanism Screening and Analysis

LUIS MIGUEL AZOFRA*[a,b] AND CHENGHUA SUN*[a,c]

[a] ARC Centre of Excellence for Electromaterials Science (ACES), School of Chemistry, Faculty of Science, Monash University, Clayton, VIC 3800, Australia; [b] Current affiliation: KAUST Catalysis Center (KCC), King Abdullah University of Science and Technology (KAUST), Thuwal 23955-6900, Saudi Arabia; [c] Faculty of Science, Engineering & Technology, Swinburne University of Technology, Hawthorn, VIC 3122, Australia
*Email: luis.azoframesa@kaust.edu.sa; chenghuasun@swin.edu.au

6.1 Introduction

Attending to the International Union of Pure and Applied Chemistry (IUPAC) Gold Book's definition of catalyst, this is ''*a substance that increases the rate of a reaction without modifying the overall standard Gibbs energy change*''.[1] The process in which a catalyst is involved receives the name of catalysis, and, depending on whether the catalytic process takes place in the same phase, or on the contrary, occurs at or near the interphase that separates two different phases, catalysis can be classified into homogeneous and heterogeneous, respectively.

Energy and Environment Series No. 21
Electrochemical Reduction of Carbon Dioxide: Overcoming the Limitations of Photosynthesis
Edited by Frank Marken and David Fermin

Published by the Royal Society of Chemistry, www.rsc.org

In this regard, Scheme 6.1 shows a schematic representation of a chemical reaction in terms of the Gibbs free energy in which reactants (R) evolve to products (P) through a first-order transition state (TS: one imaginary frequency). As indicated in (a), the presence of a catalyst decreases the activation barrier ($G_c^{\neq}$) with respect the non-catalysed process ($G_{nc}^{\neq}$), and therefore increases the rate constant of the reaction by virtue of the Arrhenius equation.[2,3] Since the catalyst participates in the process as a promoter of the reaction but it is regenerated once reactants reach products, the reaction energy (G_R) is, by definition, not affected. At the end, the negative value of the Gibbs free energy variation between products and reactants leads to a spontaneous/exergonic process for this specific instance. By contrast, (b) represents the case of a chemical reaction in which the activation barrier increases ($G_i^{\neq} > G_{ni}^{\neq}$) in the presence of what can be considered a 'negative' catalyst. This behaviour is known as inhibition, that is, a process in which "*a substance known as inhibitor decreases the rate of a reaction without modifying the overall standard Gibbs energy change*". Finally and as happened in (a), G_R remains unchanged when compared with the non-inhibited and inhibited cases, however, its positive value leads to a non-spontaneous/endergonic process for this specific example.

However, why is the concept of catalysis so important? The answer is clear. If the introduction of a catalyst during a chemical reaction decreases the activation barrier from, for instance, 1.00 to 0.25 eV, this supposes an energy saving of three quarters; the economic consequences are therefore evident, and if this energy comes from fossil fuel sources, it also means the production of just a quarter of the greenhouse gases that otherwise would have been completely emitted into the atmosphere.

Despite the fact that inhibition processes are also of paramount importance for many chemical applications, we will just focus on those chemical reactions in which $G_{nc}^{\neq} > G_c^{\neq}$ (Scheme 6.1(a)), that is, catalysis. Scheme 6.2 presents the case of a multi-step catalysed chemical reaction

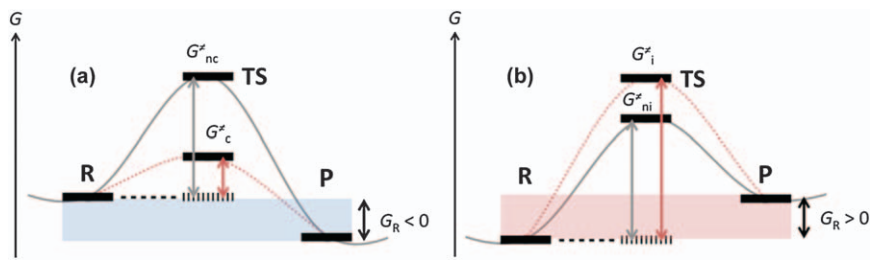

Scheme 6.1 Schematic representation of a chemical reaction in terms of the Gibbs free energy: (a) catalysed and non-catalysed; and (b) non-inhibited and inhibited. R, TS, and P refer to reactants, transition state, and products, respectively. $G^{\neq}$ and G_R refer to the Gibbs free activation and reaction energies, in each case.

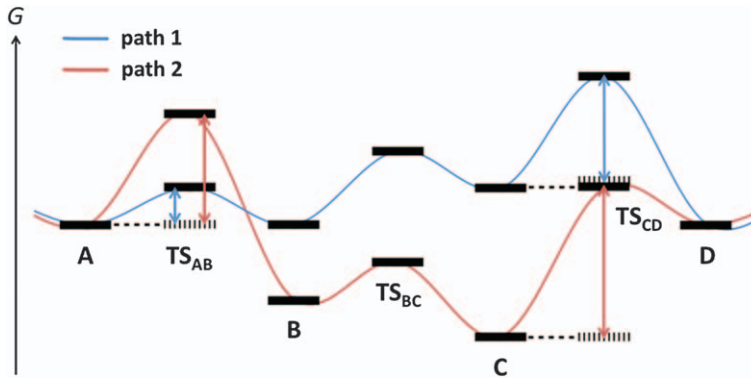

Scheme 6.2 Schematic Gibbs free energy diagram for a catalysed **A**→**D** chemical reaction following two mechanistic routes: path 1 (in blue) and path 2 (in red).

in which **A** (reactant) evolves to **D** (product) prior to passing from the **B** and **C** intermediate species and their respective TS. The use of a hypothetical catalyst leads to two different mechanistic routes, named as path 1 and path 2. First of all, it seems that an inconsistency arises with respect the formal concept of catalysis. That is, why are the reaction energies for obtaining the **B** and **C** intermediate species different when comparing both reaction mechanisms? The concept 'intermediate species' precisely refers to chemical entities existing as transitional minima or metastable structures. Since the nature of the species–catalyst interactions are different based on when they occur, therefore different thermodynamics can be seen in such cases. However, both paths obey the principle of the non-modified overall standard Gibbs energy change between products (**D**) and reactants (**A**).

Thus, at the beginning of the reaction process, **A** is converted into **B** once it has passed the respective $\mathbf{TS_{AB}}$. Despite $\mathbf{B_2}$ being thermodynamically more stable than $\mathbf{B_1}$, kinetics reveal that the activation barrier for $\mathbf{TS_{AB,\,1}}$ is lower than the one demanded when going through $\mathbf{TS_{AB,\,2}}$. This entails a majority of $\mathbf{B_1}$ intermediate species being obtained despite $G(\mathbf{B_2}) - G(\mathbf{B_1}) < 0$, *i.e.* the reaction takes place *via* the minimum energy path, being path 1 in this circumstance. Against this fact, we say that the reaction is governed by a kinetic control. Alternatively, giving the hypothetical case in which $G(\mathbf{TS_{AB,\,1}}) \geq G(\mathbf{TS_{AB,\,2}})$, undoubtedly thermodynamic control will be imposed and a majority of $\mathbf{B_2}$ species will be obtained at this stage of the reaction.

Finally, the reaction follows with obtaining $\mathbf{C_1}$ and $\mathbf{D_1}$ and their respective $\mathbf{TS_{BC,\,1}}$ and $\mathbf{TS_{CD,\,1}}$. However, since the activation barrier for the evolution of $\mathbf{C_1}$ up to $\mathbf{TS_{CD,\,1}}$ is the largest of the activation Gibbs free energies, this indicates that precisely this step becomes the limiting one of the whole process.

One of the key objectives of the quantum mechanical modelling of many-body (or *N*-body) systems is precisely the calculation of the energy. The information that can be extracted from this and its directly related properties (structural parameters, harmonic vibrational frequencies, orbitals/bands,[†] dipole moment, *etc.*) allows the hypothesising of the factors that explain the stability and reactivity of the chemical species and the role that the introduction of catalysts plays in such properties, *inter alia*. Among the variety of quantum mechanical methods at the disposal of the theoreticians' community, well-resolved density functional theory (DFT)[4] is, undoubtedly, one of the most powerful, and, therefore, widely used in the literature. In this regard:

1. DFT is based on the electron density, a physical observable.
2. DFT scales $O(N^3)$, which is much better than *ab initio* post-Hartree–Fock second-order Møller–Plesset perturbation theory [MP2, $O(N^4)$],[5] and extremely more superior than coupled clusters with singles and doubles [CCSD, $O(N^6)$],[6] for instance.
3. Multiple algorithms and approximations have been developed/implemented to decrease the time that DFT demands; this overcomes the bottleneck imposed by the $O(N^3)$ scaling, especially when the size of the system exceeds a certain number of atoms (as from a hundred).
4. On the market (commercial), and also under academic and GNU licenses, there are several tens of codes for DFT modelling.
5. And, what could be understood as a limitation of DFT, that is, the inexistence of an accurate and universal functional to the external potential, it is supplied with a wide range of general and specific functionals and the respective vast literature has been applied, even compared, to a multitude of systems.

Hence, it is not surprising to find that the DFT methodology is implemented in fields such as material sciences, and, by extension, in the *in silico* study of catalytic processes. In this regard, quantum mechanical modelling (but especially DFT due to the aforementioned strong points), allows the proposition of candidates ('initial guesses' from the theoretical formalism) to be evaluated before they are synthesised. This benefits experimentalists, who can start from those promising 'targets' previously identified by computational calculations; this can dramatically improve the success rate of materials development, and means, in the majority of cases, the saving of time and economic resources, besides offering an explanatory and complementary point-of-view of the events that occur at the atomic level. Thus, in the present chapter, we offer a comprehensive guide on DFT modelling of the catalytic carbon dioxide (CO_2) conversion mechanism into hydrocarbon compounds through the electrochemical approach.

[†]Formally, an orbital is a mathematical function that is an exact solution to the Schrödinger equation for a hydrogen-like system (H, He^+, Li^{2+}, H_2^+, *etc.*). However, the term has been improperly extended to many-body systems being widely accepted by the scientific community.

6.2 Insights into the Electrochemical CO_2 Conversion Reaction Mechanisms

Even after more than four decades of research, the development of realistic machinery for the catalytic conversion of CO_2 into hydrocarbon compounds still remains a 'hot topic'. This impact has its base in the implications that CO_2 has in the energy, environmental, biological, or industrial fields, among others. Since the beginning of the first industrial revolution to today, humanity has used non-renewable sources as the main form of energy production through the combustion of fossil fuels. In this regard, CO_2 has been a major product, and according to the National Oceanic and Atmospheric Administration (NOAA) Earth System Research Laboratory[7] its concentration in the atmosphere has reached a concerning level of 400 ppm with expectations of further rises at a rate of 2 ppm per year.[8] As result of fierce industrial activity, the role of CO_2—a natural gas with important implications for life—is clearly compromised by its consequences of the intensified greenhouse effect and climate change.[9,10] Thus, the reverse of this process is profiled as one 'green' alternative for energy consumption.[11] In this regard:

1. CO_2 is a natural source found in large quantities as a component of air.
2. The re-burning of hydrocarbon fuels as result of CO_2 conversion produces 'clean' energy since the balance of greenhouse emissions is exactly zero, always assuming that the energy provided during the conversion process comes from renewable sources.
3. The 'green' fuels generated through CO_2 conversion are easily manageable and transportable.

In nature, CO_2 is an abundant gas with a very high stability. Form the structural point-of-view, CO_2 is a linear molecule ($D_{\infty h}$ group of symmetry) with in-equilibrium R(C=O) distances equal to 1.162 Å. From an electrostatic perspective, CO_2 exhibits one electrostatic potential minimum on the 0.001 au electron density iso-surface (van der Waals iso-surface in atoms) along the C=O direction of each terminal O atom, and a set of multiple maxima surrounding the central C atom (see Figure 6.1(a)). These stationary points in the potential have been estimated to be −0.46 and 1.20 eV, respectively, at the MP2/aug-cc-pVDZ computational level, and correspond to the classical 'rabbit ear' lone pairs on O (O_{lp}) and the π-holes surrounding the sp-hybridised C of CO_2 in each case.[12]

This information revealed by the molecular electrostatic potential (MEP)[13] on the 0.001 au electron density iso-surface is of great significance since it indicates the potential role that these moieties would play when interacting with complementary moieties from partner molecules. In this regard, it advertises that O_{lp} will act as electron donor moieties with electropositive binding sites *via* presumably weak $O{=}C{=}O_{lp}\cdots X(\delta^+)$ interactions, while stronger contacts can occur with electronegative binding sites through $X(\delta^-)\cdots C(\pi\text{-hole})$ interactions, and acting C(π-hole) as an electron acceptor

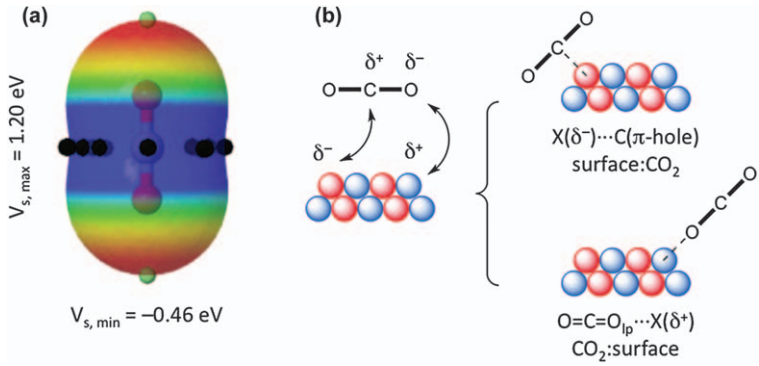

Figure 6.1 (a) MEP (±0.015 au iso-contour) on the 0.001 au electron density iso-surface for the isolated molecule of CO_2 calculated at the MP2/aug-cc-pVDZ computational level (WFA-SAS program).[14] From red to blue colours, from more negative to more positive potentials are indicated. Green and black spheres represent minima (O_{lp}) and maxima (π-holes on C), respectively. (b) Potential binding sites between CO_2 and a hypothetical surface catalyst indicating the cases in which CO_2 acts as electron acceptor or donor, respectively.

(see Figure 6.1(b)). Undoubtedly, among the variety of interactions that might take place, those of electrostatic nature will be always the most intense, although a significant dose of dispersion could also come into play.

The study of the interaction of CO_2 with partner substances is of paramount relevance since these so-called 'partners' could be the catalyst. Obviously, and as a prerequisite to start the catalytic conversion process, this cannot occur if there is no physicochemical contact between the substrate (CO_2, in this case) and the catalyst. In this sense, there are several lines of research exclusively dedicated to the description and development of novel and improved techniques for the enhancement of CO_2 adsorption as well as the search for new materials or approaches in which CO_2 could be chemisorbed[15–17] or captured.[18–20]

Once CO_2 is fixed (physi- or chemisorbed) on the catalytic surface, the reduction process takes places in successive elementary electrochemical reactions, that is, one proton (H^+) and one electron (e^-) are added to CO_2 or the immediately preceding species. Attending to the even number of H^+/e^- pairs transferred along the whole process, different hydrocarbon compounds can be obtained: carbon monoxide (CO) or formic acid (HCOOH, two), formaldehyde (H_2CO, four), methanol (CH_3OH, six), or methane (CH_4, eight). Although the possibility of the highly efficient production of CO and/or HCOOH is of great importance for chemical research, from a practical point-of-view, the low energy storage capacity of these less-reduced compounds do not make them good candidates for use in 'green' fuels technology; the amount of energy that can be obtained *via* combustion will be larger when the final product has a higher number of C–H covalent bonds and, in that sense, more reduced compounds are much more desirable.

However, which factors affect the major production of one hydrocarbon compound against the others? And, before this, how? Scheme 6.3 describes in a very clear way the different paths that isolated CO_2 can follow when reduced into CO, and HCOOH, H_2CO, CH_3OH, and CH_4 hydrocarbon compounds. Each one of these steps occurs from elementary electrochemical reactions in which one given species gains one H^+/e^- pair to further produce the hydrogenated intermediate species/product. In this sense, for the first electrochemical hydrogenation of CO_2, two options appear as separated mechanisms: on the one hand, leading to the $HOCO^\bullet$ intermediate species (eqn (6.1)), *i.e.* H is linked to one of the two O atoms from CO_2; on the other, the $OCHO^\bullet$ intermediate species is postulated (eqn (6.2)), H being linked on the C atom of CO_2:

$$CO_2 + H^+ + e^- \rightarrow HOCO^\bullet \quad (6.1)$$

$$CO_2 + H^+ + e^- \rightarrow OCHO^\bullet \quad (6.2)$$

As is clearly shown in Scheme 6.3, and obviating inter-conversion processes, the further mechanistic route depends on which radical is produced. That is, during a second H^+/e^- pair gain on the $HOCO^\bullet$ radical, three reductions might take place: (i) electrochemical hydrogenation on the previously hydrogenated O atom to reach CO and a released H_2O

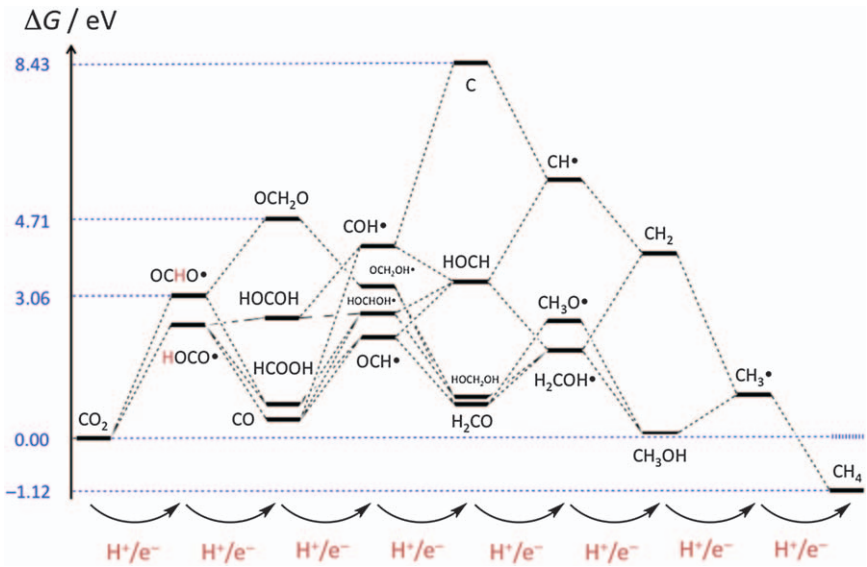

Scheme 6.3 Schematic Gibbs free energy diagram *vs.* SHE (just thermodynamics, in eV) for the electrochemical CO_2 reduction into CO, and HCOOH, H_2CO, CH_3OH, and CH_4 hydrocarbon compounds, in the gas phase and at mild conditions ($T = 298.15$ K), calculated at the MP2/aug-cc-pVTZ computational level. (Calculated through the facilities provided by the Gaussian09 package, revision D.01.)[21]

molecule; (ii) electrochemical hydrogenation on the C atom to reach HCOOH; and (iii) electrochemical hydrogenation on the non-reacted O atom to reach HOCOH. However, if the second H^+/e^- pair gain occurs on the $OCHO^\bullet$ radical, HCOOH can be also obtained if it occurs on one of the O atoms or OCH_2O if it occurs on the previously hydrogenated C atom. Obviously, HCOOH is a common product, while the CO product (plus a released H_2O molecule) and the HOCOH intermediate species can only come from the $HOCO^\bullet$ radical, or, alternatively, OCH_2O from $OCHO^\bullet$.

From here, it is found that the reaction evolves increasingly through a considerably complicated mechanism. Then, a series of multiple pathways can be postulated, as for instance, the two indicated in Scheme 6.4 and coming into play on the catalytic surface:

Thus, once the adsorbed CO_2 species is hydrogenated to reach the $HOCO^\bullet$ radical, CO (with the release of a H_2O molecule), a $HCO^\bullet$ radical, H_2CO, and a $CH_3O^\bullet$ radical are obtained along the second, third, fourth and fifth H^+/e^- pair gains, respectively. In this context, and giving a hypothetical catalytic surface in which red and pink balls represent electronegative and positive binding sites, a set of specific interactions might take place. Strong $C^\bullet\cdots X(\delta^+)$ connections between $HCO^\bullet$ and the surface are expected, or weak H-bonds between H_2CO and the $X(\delta^-)$ moiety from the material. These questions are not of trivial nature, since the specific interactions between substrate and surface could, and in fact can, define the minimum energy path. It is for that reason that, *in praxis*, delving into the interactions and the conformational exploration is of crucial importance for realistic modelling, and the conclusions which can be drawn from the thermodynamics and kinetics analysis derived from that.

Additionally, during the sixth to eighth H^+/e^- pair gains, two different mechanistic routes can be seen: on the one hand, a $CH_3O^\bullet$ radical could be reduced by formation of CH_3OH (Scheme 6.4(6a)), to finally reach CH_4 prior passing to the $CH_3^\bullet$ intermediate species (and the release of the second H_2O molecule); on the other, it is hypothesised an alternative path in which CH_4 is firstly produced (Scheme 6.4(6b)) being the catalytic surface as O-deposited, and producing the second H_2O molecule at the end of the process.

From a pragmatic point-of-view, some strategic points deserve mentioning in this context:

1. The isolated transformation of isolated CO_2 exhibits very large thermodynamic impediments. For example, the first elementary electrochemical reduction that could lead to the formation of the $HOCO^\bullet$ and $OCHO^\bullet$ radicals exhibit Gibbs free reaction energies (at MP2/aug-cc-pVTZ level) of 2.41 and 3.06 eV *vs.* SHE, respectively. It is obvious that the introduction of the catalyst is precisely based on a decrease in these impediments, describing a smother reaction route. It is for that reason that an adequate and smart idea as an initial approach is the modelling of just the clean surface, fixed CO_2, and adsorbed $HOCO^\bullet$ and $OCHO^\bullet$ radical states in order to test the Gibbs

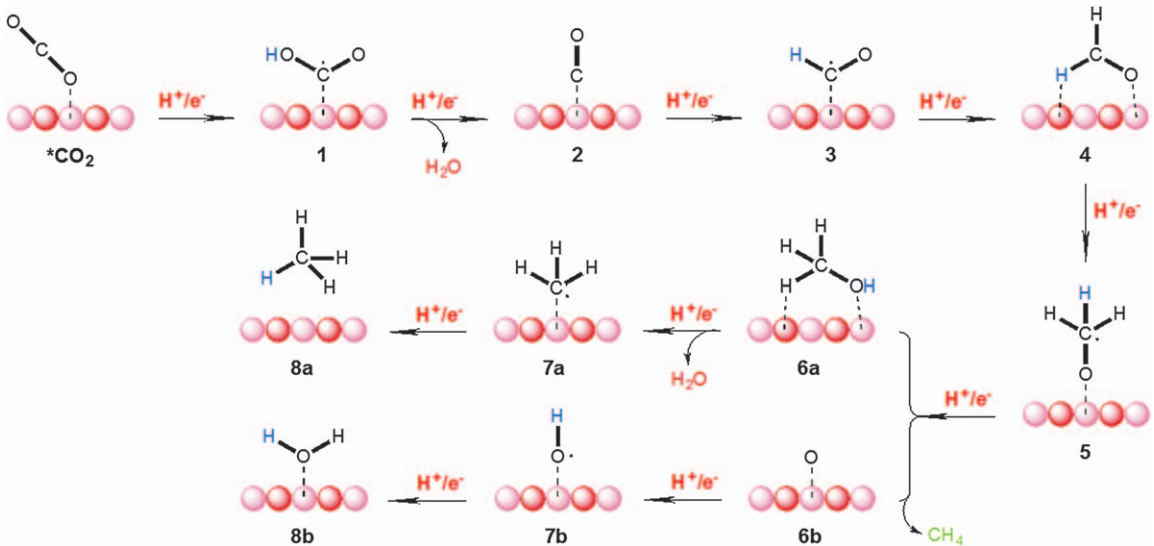

Scheme 6.4 Schematic representation for the electrochemical CO_2 conversion into the CH_4 mechanism through the CO pathway and following two different mechanistic routes from the fifth H^+/e^- pair gain. Red and pink balls represent electronegative and positive binding sites for a hypothetical catalytic surface material, respectively. Introductions of new H^+/e^- pairs are highlighted in blue.

free binding energy of CO_2 and the reaction Gibbs free energies due to the first electrochemical hydrogenation steps. If the test results are positive, that is, if a low reaction energy is obtained, it would be essential to estimate the activation barriers for both $HOCO^{\bullet}$ and $OCHO^{\bullet}$ radical formation.

2. Strongly related to this, it is well known that the electro-reduction of isolated CO_2 demands a very high potential, −1.90 V *vs.* NHE (eqn (6.3)),[22] and the first electrochemical hydrogenation represents the largest impediment, limiting the step of the overall process. This is also very usual when catalysed, and, once located, which is the step corresponding to the minimum energy path ($HOCO^{\bullet}$ *vs.* $OCHO^{\bullet}$ radicals), the mechanism is greatly simplified.

$$CO_2 + e^- \rightarrow CO_2^{\bullet -}, \qquad \varepsilon^0 = -1.90 \text{ V } \textit{vs.} \text{ NHE}. \tag{6.3}$$

3. Also, one might assume that we will not find, except in special cases, Gibbs free energies (both reaction and activation values) much larger during the successive H^+/e^- pair gains. This leads us to conclude that a comprehensive, accurate prediction of the thermochemistry during the early CO_2 fixation and first electrochemical hydrogenation steps generally represents a good approximation of the limitations imposed by the selected material.

Finally, very close potentials are seen for the CO and hydrocarbon compounds obtained during the CO_2 reduction (eqn (6.4)–(6.8)). However, the catalytic surface imposes the selectivity. Thus, following the minimum energy path can be hypothesised by the major product that would be obtained.

$$CO_2 + 2H^+ + 2e^- \rightarrow CO + H_2O, \qquad \varepsilon^0 = -0.61 \text{ V} \tag{6.4}$$

$$CO_2 + 2H^+ + 2e^- \rightarrow HCOOH, \qquad \varepsilon^0 = -0.53 \text{ V} \tag{6.5}$$

$$CO_2 + 4H^+ + 4e^- \rightarrow H_2CO + H_2O, \qquad \varepsilon^0 = -0.48 \text{ V} \tag{6.6}$$

$$CO_2 + 6H^+ + 6e^- \rightarrow CH_3OH + H_2O, \qquad \varepsilon^0 = -0.38 \text{ V} \tag{6.7}$$

$$CO_2 + 8H^+ + 8e^- \rightarrow CH_4 + 2H_2O, \qquad \varepsilon^0 = -0.24 \text{ V}. \tag{6.8}$$

6.3 Thermochemistry and Chemical Kinetics in Electrochemical Reactions[‡]

In theoretical chemistry, there are three widely used energy quantities that provide very useful, specific information for the understanding of the physicochemistry during a chemical (catalysed or not) reaction. We refer to the

[‡]A basic understanding of fundamental concepts in quantum mechanics, physical chemistry and statistical mechanics is assumed.

electronic energy (E), the enthalpy (H), and the Gibbs free energy (G). Negative changes in E, H, and G lead to favoured, exothermic, and spontaneous/exergonic processes, respectively, while positive values indicate non-favoured, endothermic, and non-spontaneous/endergonic processes, respectively. From the fundamental relations of thermodynamics it is inferred that:

$$G^0 = H^0 - TS \tag{6.9}$$

where G^0 and H^0 refer to the standard Gibbs free energy and enthalpy, and T and S denote temperature and entropy. At temperatures greater than 0 K and constant pressure (for mild conditions, $T = 298.15$ K), enthalpy can be expressed in terms of H^0 and the heat capacity, C_P:

$$H = H^0 + \int C_P \, dT. \tag{6.10}$$

In addition, the entropy term can be expressed as the sum of the translational, rotational, vibrational, and electronic contributions as to:

$$S = S_t + S_r + S_v + S_e. \tag{6.11}$$

And therefore:

$$G = H^0 + \int C_P \, dT - T(S_t + S_r + S_v + S_e). \tag{6.9}$$

AQ:1 In addition to these formal quantities, two additional correction terms can be added to eqn (6.9): on the one hand, and of intrinsic nature, the vibrational zero-point energy (ZPE); on the other hand, extrinsic dispersion (D) corrections (the explicit formulae of D depends on the method employed):

$$G = H^0 + \int C_P \, dT - T(S_t + S_r + S_v + S_e) + \mathrm{ZPE} + D \tag{6.9}$$

$$\mathrm{ZPE} = \frac{1}{2}\sum h\nu_i \tag{6.12}$$

ν_i being each one of the $3N-6$ ($3N-5$ in isolated linear molecules) vibrational frequencies. Thus, the Gibbs free energy variation (relative Gibbs free energy) between two different states, 2 and 1, for a given system, can be expressed as follows:

$$\begin{aligned}\Delta G_{21} = G_2 - G_1 = {} & H_2^0 + \int C_{P,\,2} \, dT - T(S_{t,\,2} + S_{r,\,2} + S_{v,\,2} + S_{e,\,2}) \\ & + \mathrm{ZPE}_2 + D_2 - H_1^0 - \int C_{P,\,1} \, dT + T(S_{t,\,1} + S_{r,\,1} + S_{v,\,1} + S_{e,\,1}) \\ & - \mathrm{ZPE}_1 - D_1\end{aligned} \tag{6.13}$$

or simply:

$$\Delta G_{21} = G_2 - G_1 = \Delta H_{21}^0 + \Delta \int (C_P)_{21} \, dT - T\Delta S_{21} + \Delta \mathrm{ZPE}_{21} + \Delta D_{21}. \tag{6.13}$$

For the specific case of the heterogeneous catalytic electrochemical CO_2 conversion mechanisms, three different energy changes are usually calculated. The first one refers to the CO_2 adsorption on the surface, and it is also known as binding energy. Thus, the chemical equation representing the

adsorption of $CO_2(g)$ (or to simplify, just CO_2) on a given surface (denoted as '*') is expressed as:

$$* + CO_2 \rightarrow *CO_2. \tag{6.14}$$

This, which is formally a chemical reaction, exhibits a Gibbs free energy variation between the product (adsorbed CO_2) and reactants (clean surface plus isolated CO_2) representing the aforementioned binding Gibbs free energy. If it is positive, the adsorption is spontaneously produced, *i.e.* no energy injection is needed. By contrast, if it is negative, it means that fixation is non-spontaneous and additional energy (pressure) is required to enhance such contact. Thus:

$$\Delta G = G_b = G(*CO_2) - G(*) - G(CO_2) \tag{6.15}$$

where:

$$G(*CO_2) = H^0(*CO_2) + \int C_P(*CO_2)\ dT - T[S_t(*CO_2) + S_r(*CO_2) + S_{v,}(*CO_2) + S_e(*CO_2)] + ZPE(*CO_2) + D(*CO_2) \tag{6.16}$$

$$G(*) = H^0(*) + \int C_P(*)\ dT - T[S_t(*) + S_r(*) + S_{v,}(*) + S_e(*)] + ZPE(*) + D(*) \tag{6.17}$$

$$G(CO_2) = H^0(CO_2) + \int C_P(CO_2)\ dT - T[S_t(CO_2) + S_r(CO_2) + S_{v,}(CO_2) + S_e(CO_2)] + ZPE(CO_2) + D(CO_2). \tag{6.18}$$

For these last equations, some approximations can be applied:

1. At the fundamental electronic level: $S_e \approx 0$.
2. For gases,[§] translational, rotational, and vibrational entropy terms have contributions that might not be neglected. Therefore: $S = S_t + S_r + S_v$.
3. For solids and adsorbates, both $S_t \approx 0$ and $S_r \approx 0$. Therefore: $S = S_v$.
4. Since $\int C_P\ dT$ is almost negligible and $\Delta \int C_P\ dT \approx 0$, no thermal corrections for the enthalpy can be taken into account.

Finally, eqn (6.16)–(6.18) can be approximated as:

$$G(*CO_2) = H^0(*CO_2) - TS_{v,}(*CO_2) + ZPE(*CO_2) + D(*CO_2) \tag{6.16}$$

$$G(*) = H^0(*) - TS_{v,}(*) + ZPE(*) + D(*) \tag{6.17}$$

$$G(CO_2) = H^0(CO_2) - T[S_t(CO_2) + S_r(CO_2) + S_{v,}(CO_2)] + ZPE(CO_2) + D(CO_2). \tag{6.18}$$

This can be also extended to the calculation of the Gibbs free reaction energy once $*CO_2$ starts to be reduced through the gain of a set of H^+/e^- pairs. The

[§]See foundations in *Quantum Chemistry*, D. A. McQuarrie and M. Hanson, Macmillan Education, 2nd revised edition, 2007.

chemical equation for the first H^+/e^- pair gain leading to the $*OCHO^\bullet$ radical species obeys:

$$*CO_2 + H^+ + e^- \rightarrow *OCHO^\bullet. \tag{6.2}$$

In view of what was previously discussed concerning the calculation of the binding Gibbs free energy, it seems obvious how $G(*OCHO^\bullet)$ and $G(*CO_2)$ can be expressed as sum of the enthalpy, entropy, ZPE, and dispersion terms. However, a fundamental question arises: which is the Gibbs free energy of the $H^+/e^-(aq)$ (or just H^+/e^-) pair? In this context, the chemical potential of the H^+/e^- pair has the half value of the chemical potential of the dihydrogen molecule, $H_2(g)$, (or just H_2, see eqn (6.19)) when working at standard hydrogen electrode (SHE) conditions, *i.e.* $f(H_2) = 101\,325$ Pa, and $U = 0$ V, being $f(H_2)$, and U the fugacity of H_2 and the external potential applied, respectively:

$$\mu(H^+/e^-) = \tfrac{1}{2}\,\mu(H_2). \tag{6.19}$$

Then:

$$\begin{aligned}\Delta G = G_R &= G(*OCHO^\bullet) - G(*CO_2) - G(H^+ + e^-) \\ &= G(*OCHO^\bullet) - G(*CO_2) - \tfrac{1}{2}\,G(H_2).\end{aligned} \tag{6.20}$$

Ultimately, the reaction Gibbs free energy to any step of the electrochemical CO_2 conversion mechanism, where n is the number of H^+/e^- pairs transferred and m the number of $H_2O(g)$ (or just H_2O) molecules released, if applicable, results in:

$$\begin{aligned}\Delta G = G_R = G(*CO_{2-m}H_{n-2m}) + m\;G(H_2O) - G(*) - G(CO_2) \\ -n/2\;G(H_2).\end{aligned} \tag{6.21}$$

Obviously, for $n = 0$ and $m = 0$, $G_R = G_b$, that is, the binding Gibbs free energy.

Some observations deserve mentioning in this context:

1. Eqn (6.19) can be only applied in the Gibbs free energy regime.
2. Despite eqn (6.19) being delimited to SHE conditions, pH corrections can be applied by inclusion of the 2.303 RT pH quantity. (For pH = 0, natural hydrogen electrode (NHE) conditions, it is obvious that 2.303 RT pH = 0.)
3. The effect of an additional external potential can be added to the calculation of the Gibbs free energy values by inclusion of the $-eU$ term. At SHE/NHE conditions, $U = 0$ V.
4. As solution of the Schrödinger equation, quantum mechanical modelling codes usually provide the electronic energy. Formally, the electronic energy only refers to the electronic part (kinetic and potential electronic energies), however, the nuclear part (just as function of the nuclei positions attending to the Born–Oppenheimer approximation) and the thermal corrections to the electronic energy are assumed to be included in the 'electronic energy' expression.

5. The relation between the electronic energy and the enthalpy, taking into account the assumption previously commented on about E, is:

$$H = E + k_B T \tag{6.22}$$

therefore $\Delta H = \Delta E$. It is for this reason that, *in praxis*, ΔH is directly estimated as ΔE.

Finally, the computation of electrochemical activation energies or barriers is a challenging topic in which important efforts have been recently reported by Janik and co-workers[23,24] in the development of a strong, founded methodology in which an inner-sphere Marcus mechanism is assumed. In classical chemical reactions, the TS is located with a zero charge–electron balance during the chemical process. In the case of elementary electrochemical reactions, a chemical species A, fixed on a catalytic surface (then, *A), gains one proton (H^+) from the bulk medium and one electron (e^-) travelling through the catalyst, in order to produce an adsorbed *AH$^\bullet$ intermediate state:

$$*A + H^+ + e^- \rightarrow *AH^\bullet. \tag{6.23}$$

Given the obvious difficulties with the location of the TS in such an elementary electrochemical reaction, Janik and co-workers proposed a location of the analogous hydrogenation (chemical) reaction in which both the *A and *H$^\bullet$ species are fixed on the surface and react in order to produce the *AH$^\bullet$ intermediate state:

$$*A + *H^\bullet \rightarrow *AH^\bullet. \tag{6.24}$$

Once located, the TS for this chemical reaction and the TS for the electro-reduction of *A can be assumed as identical at one specific electrode potential, U_0, *i.e.* U_0 equates the energy of the $*A + *H^\bullet$ reactants to $*A + H^+ + e^-$, as shown in the schematic parabolic curves approximated by the Marcus theory (Scheme 6.5):

Finally and attending to the Butler–Volmer theory, the Gibbs free activation barrier of the electro-reduction of *A, $G^{\neq}$, can be approximated as:

$$G^{\neq}(U) = G^{\neq 0} + \beta F(U - U_0) \tag{6.25}$$

where $G^{\neq 0}$ is the activation barrier for the hydrogenation reaction of *A, β the symmetry coefficient (and approximated to 0.5), F the Faraday constant, and U the applied electrode potential.

6.4 In Practice

In the present section, practical aspects for the well-resolved DFT modelling of the catalysed electrochemical mechanisms of CO_2 will be treated. In this regard, a few points deserve overall consideration before starting:

1. As fundamental requisite for the existence of catalysis, it is evident that a 'catalyst' should be considered. But how to know whether a material

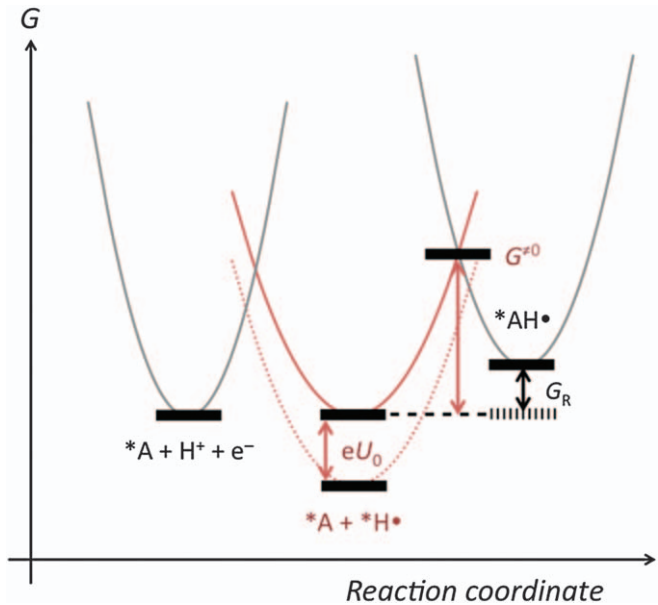

Scheme 6.5 Schematic representation of Marcus curves for the $^*A + H^+ + e^-$, $^*A + {}^*H^\bullet$, and $^*AH^\bullet$ species.

will act as a catalyst or not? Through an analysis of specific elements, such as the atoms' connectivity, potential electrostatic binding-points, or selective reactivity, amongst others, it is possible to propose promising candidates.

2. The selection of the methodology plays a key role. An inadequate theoretical treatment might lead to unrealistic outcomes, either false or positive-negative results.
3. Since the theoretical DFT modelling is carried out thanks to the facilities provided by a software program, it is essential to have a broad knowledge of the function, settings, and theoretical basis with which such a program works.
4. Last, but not least, in many of the cases the use of a significant amount of computational resource is required. In this sense, it should be noted that most of the calculations demand computational time that simply exceeds the limits of a personal computer, even of small clusters used for the modelling of small-size systems or dedicated to performing tests.

Answering these questions:

1. As a catalyst, our choice is the (001) surface of anatase titanium dioxide, TiO_2.
2. As a methodology, we use well-resolved DFT through the generalised gradient approximation (GGA) with the Perdew–Burke–Ernzerhof (PBE)

functional[25] and employ explicit dispersion corrections through the use of the D3 method with the standard parameters programmed by Grimme and co-workers.[26,27]

3. As a simulation program, we employ the facilities provided by the Vienna *Ab-Initio* Simulation Package (VASP, version 5.3.5).[28–31]
4. All calculations were carried out at the National Computational Infrastructure (NCI), which is supported by the Australian Government.

Thus, anatase TiO_2(001) is constituted, in such specific surface, by two kind of O atoms: two-fold or coordinated (labelled as 2c-O in Figure 6.2) and three-fold (3c-O) atoms, being the first the highest reactive (since 3c-O atoms are electronically saturated) for its plausible interactions with positive moieties from partner molecules. Also, all Ti atoms are in the form of five-fold (5c-Ti) atoms, presenting the ability to be potentially bound with negative moieties from partner molecules.

Before carrying out any modelling, the catalyst cell should be build and optimised. For the case of materials with crystal structure, it is possible and convenient to use experimental data provided by the various crystallography databases, many of them of with free access. In the case at hand (see Figure 6.2), the unit cell of anatase TiO_2 was downloaded, expanded, and cut in order to produce a $3\times3\times5$ super-cell of anatase TiO_2 ($Ti_{45}O_{90}$) in which the (001) surface pointed towards the *OZ* axis, and the (100) surface pointed towards the *OX* and *OY* axes.

Once the super-cell is built, it is required to proceed with the optimisation of the lattice parameters defined throughout the $\boldsymbol{a}$, $\boldsymbol{b}$, and $\boldsymbol{c}$ vectors. As a practical hint, it is quite desirable to centre the *OX* and *OY* positions in order to avoid change in the relative positions of the atoms as well as to prevent the same for the *OZ* positions moving the super-cell a sufficiently reasonable amount with respect the $z = 0$ plane.

The cell parameters for anatase TiO_2(001) constitute a triclinic (3D) lattice system, being the cell angles $\alpha = \beta = \gamma = 90^\circ$ and the $|\boldsymbol{a}|$ and $|\boldsymbol{b}|$ cell length

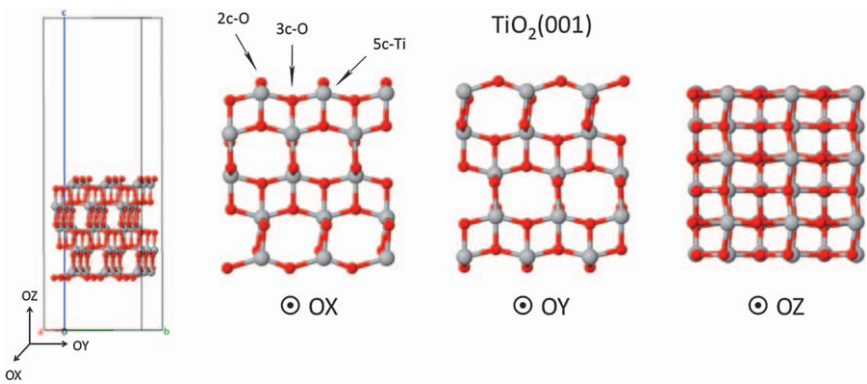

Figure 6.2 From left to right: (001) surface (*OZ*) for a $3\times3\times5$ super-cell of TiO_2 ($Ti_{45}O_{90}$) and its *OX*, *OY*, and *OZ* perspectives.

modules equal to 11.328 Å for this specific case. Since the (001) surface is expressed through the *OZ* axis, it represents a cutting in the crystal structure. For this reason, it is imposed that $|\boldsymbol{c}| = 35$ Å, and a vacuum distance of around 25 Å is supposed to avoid interactions between periodic images.

In the VASP environment, four files need to be prepared:[32]

1. POSCAR: containing the cell parameters, atom types and their quantity, and direct lattice coordinates (eventually, also forces if data were provided in a previous calculation).
2. POTCAR: containing the plane-wave pseudo-potentials. In the case at hand, projected augmented-wave (PAW) PBE pseudo-potentials: Ti (PAW_PBE Ti 08Apr2002) and O (PAW_PBE O 08Apr2002) for TiO_2, and also C (PAW_PBE C 08Apr2002) and H (PAW_PBE H 15Jun2001), which will be required later for the modelling of the CO_2 conversion.
3. KPOINTS: containing, in this case, representative $3\times3\times1$ *k*-points following the Monkhorst–Pack scheme and having been tested before with a larger set of *k*-points to make sure that there were no significant changes in the calculated energies.
4. INCAR: containing the settings for the modelling. Here, well-resolved DFT through: (i) a GGA-PBE functional; (ii) plane-wave cut-off energy of 450 eV;[33,34] (iii) energy and force convergence limits equal to 10^{-4} eV per atom and $|0.02|$ eV Å^{-1}, respectively; (iv) Gaussian smearing for the f_{nk} partial occupancies set for each wavefunction; (v) 0.02 eV for the width of the smearing; (vi) a conjugate gradient algorithm; (vii) 0.2 fs for the scaling constant of the forces; (viii) explicit D3 dispersion corrections; and (ix) the rest of the by-default settings.

Once the required accuracy was reached, that is, once it was optimised, VASP provides a total electronic energy ('TOTEN' in the VASP formalism) of −1194.74 eV. This optimisation is just the optimised structure for a given lattice parameters and does not mean that it is the optimum. The lattice parameters should be optimised as well, and for that reason, eqn (6.26) to (6.28) should be applied in order to search those lattice parameters that lead to the minimum energy. The χ factor just expands (if $\chi>1$) or contracts (if $\chi<1$) the cell. It is assumed that at the beginning, $\chi = 1.00$ (at the top of the INCAR file) was used. Then, with an accuracy in the hundredths, we can obtain the TOTEN when $\chi = 1.01$ (expansion) and $\chi = 0.99$ (contraction) but always keeping the same value of $|\boldsymbol{c}|$ to proceed with a consistent comparison:

$$\boldsymbol{a} = \chi\boldsymbol{a_x} + \chi\boldsymbol{a_y} + \chi\boldsymbol{a_z} = \chi\boldsymbol{a_x} = \chi \cdot 11.328\boldsymbol{i} \tag{6.26}$$

$$\boldsymbol{b} = \chi\boldsymbol{b_x} + \chi\boldsymbol{b_y} + \chi\boldsymbol{b_z} = \chi\boldsymbol{b_y} = \chi \cdot 11.328\boldsymbol{j} \tag{6.27}$$

$$\boldsymbol{c} = \chi\boldsymbol{c_x} + \chi\boldsymbol{c_y} + \chi\boldsymbol{c_z} = \chi\boldsymbol{c_z} = 35\boldsymbol{k}, \text{ in all cases.} \tag{6.28}$$

Table 6.1 TOTEN (in eV) along the optimisation of the lattice parameters of the $Ti_{45}O_{90}$ super-cell of $TiO_2(001)$.

	χ	TOTEN
↑	1.01	−1194.74
→	1.00	−1195.31
↓	**0.99**	−1195.52
↑	0.98	−1195.45

Results (see Table 6.1) indicate that TOTEN($\chi = 1.01$) > TOTEN($\chi = 1.00$), and TOTEN($\chi = 0.99$) < TOTEN($\chi = 1.00$). This leads us to conclude that it is still required to contract the cell up to find the minimum electronic energy. Finally, since TOTEN($\chi = 0.98$) > TOTEN($\chi = 0.99$), it is evident that for $\chi = 0.99$ the optimised lattice parameters can be found, being $|\boldsymbol{a}| = |\boldsymbol{b}| = 11.215$ Å and $|\boldsymbol{c}| = 35$ Å.

Here, a fundamental question still arises: does the methodology employed represent well the crystal structure and properties of $TiO_2(001)$? As can be seen, the optimised lattice parameters and, then, the optimised structure from this turn out to be very close to the crystal structure, with similar O–Ti covalent distances between the experimentally measured and the theoretically predicted, and exhibiting a good agreement of the band gap when a HSE06 (Heyd–Scuseria–Ernzerhof functional)[35–37] single point calculation over the PBE optimised geometry was carried out. Thus, the methodology can be considered as validated.

The next step consists in the analysis of the CO_2 interactions on the $TiO_2(001)$ surface as fundamental prerequisite to start the catalytic process. In this regard, it seems evident that there is no catalysis if both surface and substrate do not present physicochemical contact. Since the calculation of the Gibbs free binding energy previously shown in eqn (6.15) consists in the subtraction of the Gibbs free energy of the CO_2:$TiO_2(001)$ complex minus the Gibbs free energy of the isolated moieties, their calculation is required.

At the present time, we have obtained the TOTEN and the associated optimised lattice parameters and structure of the clean $TiO_2(001)$ surface. How to calculate, *in praxis*, the Gibbs free energy? For this purpose, it is required a second calculation with the following details:[32]

1. POSCAR: the previously optimised structure contained in the CONTCAR file.
2. POTCAR: the same as in the previous case.
3. KPOINTS: since it is necessary carry out a vibrational/phonon frequency analysis, this is only possible to do for Γ points, that is, 1×1×1 *k*-points following the Monkhorst–Pack scheme. Once done, a set of vibrational/phonon frequencies appear and, eventually, also a set of imaginary low values. They are associated with vibrational motions in the margins/limits of the cell and as result of the cutting to Γ points.

4. INCAR: in this case, a single-point calculation will be performed with the following parameters: (i) along the ionic and electronic relaxations, the same parameters can be used, although a more accurate precision setting can be chosen; (ii) if dispersion corrections were previously carried out, they should also be included here; and (iii) for the calculation of vibrational/phonon frequencies, the finite differences method is applicable in order to determine the second derivatives throughout the Hessian matrix. It is important to note that the number of iterations done to reach a self-consistent field (SCF) should be lower than the maximum number of iterations programmed. Otherwise, the results can develop into energy artefacts/inaccuracies because the SCF has not been reached. Also, it is recommended that a minimum of 6–8 iterations per alteration during the finite differences calculation should be carried out.

From these sets of calculations the Γ points can be extracted: the total electronic energy (and then, enthalpy), which directly includes the dispersion corrections, the entropy contributions, and the ZPE. However, there are different strategies concerning the selection of TOTEN. Some authors include the thermal and vibrational terms to obtain the Gibbs free energy from the TOTEN with the largest set of *k*-points, others choose the value directly obtained from the Γ points. In this case, we are working with the second case. As an important hint, it is quite important to take into account that, in the first case, the TOTEN that should be selected is the last one before reaching the required accuracy, while in the second it should be the first one after reaching the SCF since it is a single-point calculation. It is true that for an *N*-atoms system, there appear $3 \cdot 2 \cdot N + 1$ iterations with their respective TOTEN. As we stated before, the first one corresponds to the single point calculation, while the rest, $3 \cdot 2 \cdot N$, carry out the alteration of each atom in the three directions (positive and negative) to evaluate the energy corresponding to each $3N$ vibrational/phonon frequency.

Table 6.2 gathers the energy quantities for the isolated H_2 and CO_2 molecules. Also, it is quite common see authors who prefer to use data from the optimised geometries of these small molecules, while others proceed with single-point calculations over the experimentally measured geometries, which are very well known due to the high precision of the detection methods in the gas phase. Also, we are working with the second case.

Table 6.2 Energy quantities for the isolated H_2 and CO_2 molecules. Experimental values from the NIST database (http://cccbdb.nist.gov): H_2 (*g*): $d_{HH} = 0.741$ Å, $\nu_1(\Sigma_g) = 4401\ cm^{-1}$; CO_2 (*g*): $d_{CO} = 1.162$ Å, $A_{OCO} = 180.0^\circ$, $\nu_1(\Sigma_g) = 1333\ cm^{-1}$, $\nu_2(\Sigma_u) = 2349\ cm^{-1}$, $\nu_3(\Pi_u) = 667\ cm^{-1}$.

Species	$E + D$	$-TS_t$	$-TS_r$	$-TS_v$	ZPE	G
H_2 (*g*)	−6.77	−0.35	−0.04	0.00 (0)	0.27	−6.89
CO_2 (*g*)	−22.92	−0.47	−0.17	−0.00 (5)	0.27	−23.29

Unlike the previous cases in which the initial geometries are almost trivial, searching for the optimised CO_2 : TiO_2(001) complexes is much more complicated since it requires an initial approach in order to propose initial structures (guesses in the theoretical formalism) as close to the real minima. This not only facilitates the convergence process and saves computational time, but also could produce real but secondary minima in stability. The consequences of this are evident and the experience here usually plays an important role.

Thus, since 5c-Ti atoms are electron-poor moieties that exhibit one electropositive vacancy, it seems reasonable that this can interact with the O lone pairs (O_{lp}) from CO_2, which are electron-rich moieties. This means plausible OCO···Ti interactions being CO_2 physisorbed on the surface. Also, another option is that 2c-O atoms in TiO_2(001), which are more reactive than 3c-O ones, could interact with the π-holes from C in CO_2 in order to physically fix both moieties through an O···CO_2 interaction. Alternatively, a secondary OCO···Ti interaction could take place in this case. Finally, the last option is that CO_2 could be chemisorbed on the surface, being in this case strong interactions in which both moieties are closer to being covalently bound than in the form of weak interactions, as in the two previous assumptions.

Effectively, such initial guesses were good representative structures of the real minima, as shown in Figure 6.3. Concerning the stability analysis, while

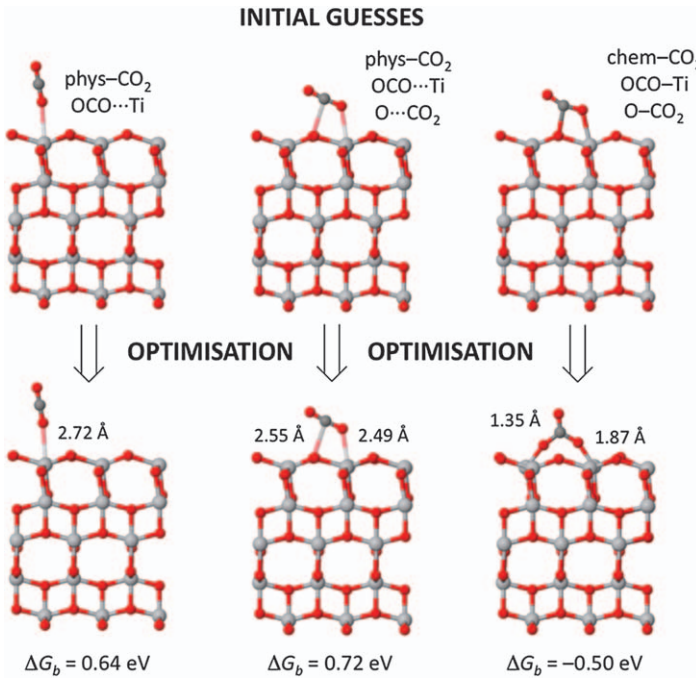

Figure 6.3 Initial structures and their corresponding optimised minima for the CO_2 fixation (physi- and chemisorbed) on TiO_2(001).

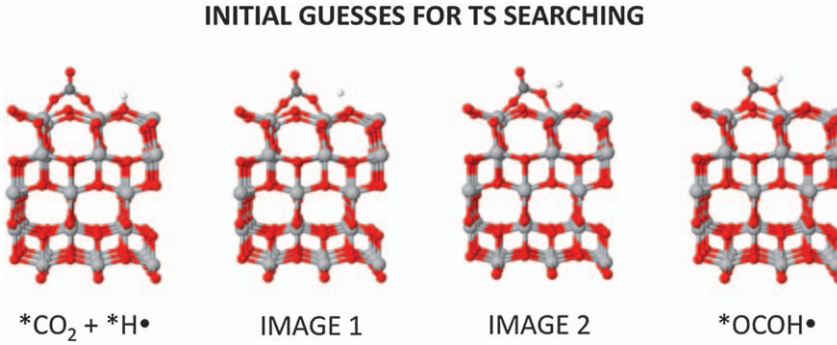

Figure 6.4 $*CO_2 + *H^{\bullet}$ and $*OCOH^{\bullet}$ minima and the proposed two NEB images (1 and 2) for searching for the TS corresponding to the first H^+/e^- pair transfer on $TiO_2(001)$. This is an illustrative calculation; a larger number of images might be necessary for a more accurate description of the TS.

physisorbed minima exhibit non-spontaneous Gibbs free binding energies (0.64 and 0.72 eV), the chemisorption of CO_2 is profiled as being more stable with a spontaneous $\Delta G_b = -0.50$ eV. For this chemisorbed state we say that CO_2 is captured on the $TiO_2(001)$ surface. It deserves to be mentioned that, at this step, searching for the TS due to the change between physisorbed and chemisorbed CO_2 might be convenient, although the barrier of this process is expected to be lower than the ones that will be computed during the further conversion processes.

Once CO_2 is chemisorbed on the surface, the next step consists in the introduction of the first H^+/e^- pair. Between the two options of $OCHO^{\bullet}$ and $OCOH^{\bullet}$ radicals, we are going to focus on the second case. Thus, the optimised structure results in the one represented on the right of Figure 6.4. Applying eqn (6.21), the reaction Gibbs free energy at 298.15 K for this is hypothesised to be -0.32 eV *vs.* NHE, that is, the process is spontaneous. However, what happens to the activation barrier? According to eqn (6.25), a description of the $*CO_2 + *H^{\bullet}$ state is required, and therefore the TS between this and the $*OCOH^{\bullet}$ radical. For this purpose, the nudge elastic band (NEB)[38] method was applied, despite there being other approaches for the location of the TS.

Finally, it is hypothesised (see Table 6.3) that the activation barrier for the electrochemical H^+/e^- pair injection from $*CO_2$ to $*OCOH^{\bullet}$ is 0.85 eV *vs.* NHE. This search should be done for all successive elementary steps in order to discriminate between the kinetic or thermodynamic controls of the reaction and locate the minimum energy path. Once the whole picture is gained, it is possible to conjecture the selectivity of the $TiO_2(001)$ surface towards the preference of one product against another and also hypothesise the maximum energy demanded for the whole process. If any larger barrier appears, once CO_2 is captured on the $TiO_2(001)$ surface, DFT advances that it

Table 6.3 Energy quantities (in eV, U_0 in V) for the calculation of the activation barrier for the first H^+/e^- pair injection from $*CO_2$ to $*OCOH^\bullet$.

Species	G	U_0	G^0_{act}	G_{act}
$*CO_2 + H^+ + e^-$	−1221.02			
$*CO_2 + *H^\bullet$	−1220.83			
TS	−1220.08	−0.19	0.75	0.85
$*OCOH^\bullet$	−1220.84			

is possible convert CO_2 into a certain hydrocarbon compound with a maximum energy input of 0.85 eV *vs.* NHE.

In summary, we have provided a set of computational tools to analyse the reaction mechanisms for the electrochemical CO_2 conversion into 'green' fuels through: (i) DFT characterisation of the material; (ii) finding structure/reactivity patterns; and (iii) estimation of the thermodynamics and kinetics of the reactions. In simpler words, providing a comprehensive guide in which we, as theoreticians, would be able to hypothesise promising candidate(s) for CO_2 conversion and deepening the understanding of the mechanistic events taking place at the atomic/electronic level. Our efforts are added to those already carried out by dozens of theoretical groups, not only on this specific topic,[39–44] but also in many other modelling studies such as hydrogen[45–50] and oxygen[51–56] evolution reactions (HER, OER) in water splitting or N_2 conversion into ammonia,[57,58] as some remarkable instances in which the foundations of this guide can be also applied. We are confident that the didactic point-of-view offered in this chapter will be of help to those researchers being introduced to the DFT modelling of heterogeneous catalysis materials chemistry and will serve as a basis to establishing a common methodology that takes into account both thermodynamic and kinetic evaluations with the aim of successful prediction and explanation.

Acknowledgements

The authors acknowledge the Australian Research Council (ARC) and the ARC Centre of Excellence for Electromaterials Science (ACES) for their support. Gratitude is also due to the National Computational Infrastructure (NCI) for providing the computational resources.

References

1. IUPAC Compendium of Chemical Terminology, Electronic version, http://goldbook.iupac.org/C00876.html.
2. S. A. Arrhenius, *Z. Phys. Chem.*, 1889, **4**, 96.
3. S. A. Arrhenius, *Z. Phys. Chem.*, 1889, **4**, 226.
4. P. Hohenberg and W. Kohn, *Phys. Rev.*, 1964, **136**, B864.
5. C. Møller and M. S. Plesset, *Phys. Rev.*, 1934, **46**, 618.
6. P. J. Knowles, C. Hampel and H. J. Werner, *J. Chem. Phys.*, 1993, **99**, 5219.

7. National Oceanic and Atmospheric Administration (NOAA) Earth System Research Laboratory, http://www.noaa.gov.
8. E. J. Maginn, *J. Phys. Chem. Lett.*, 2010, **1**, 3478.
9. T. R. Karl and K. E. Trenberth, *Science*, 2003, **302**, 1719.
10. J. Meyer, *Nature*, 2008, **455**, 733.
11. D. T. Whipple and P. J. A. Kenis, *J. Phys. Chem. Lett.*, 2010, **1**, 3451.
12. L. M. Azofra, *Chem. Phys.*, 2015, **453–454**, 1.
13. J. S. Murray and P. Politzer, *WIREs Comput. Mol. Sci.*, 2011, **1**, 153.
14. F. A. Bulat, A. Toro-Labbé, T. Brinck, J. S. Murray and P. Politzer, *J. Mol. Model.*, 2010, **16**, 1679.
15. Q. Sun, Z. Li, D. J. Searles, Y. Chen, G. Lu and A. Du, *J. Am. Chem. Soc.*, 2013, **135**, 8246.
16. X. Meng, S. Ouyang, T. Kako, P. Li, Q. Yu, T. Wang and J. Ye, *Chem. Commun.*, 2014, **50**, 11517.
17. H. Kiuchi, R. Shibuya, T. Kondo, J. Nakamura, H. Niwa, J. Miyawaki, M. Kawai, M. Oshima and Y. Harada, *Nanoscale Res. Lett.*, 2016, **11**, 127.
18. X. Zhang, X. Zhang, H. Dong, Z. Zhao, S. Zhang and Y. Huang, *Energy Environ. Sci.*, 2012, **5**, 6668.
19. M. Vogt, J. E. Bennett, Y. Huang, C. Wu, W. F. Schneider, J. F. Brennecke and B. L. Ashfeld, *Chem. – Eur. J.*, 2013, **19**, 11134.
20. C. Kunkel, F. Vines and F. Illas, *Energy Environ. Sci.*, 2016, **9**, 141.
21. M. J. Frisch, G. W. Trucks, H. B. Schlegel, G. E. Scuseria, M. A. Robb, J. R. Cheeseman, G. Scalmani, V. Barone, B. Mennucci, G. A. Petersson, H. Nakatsuji, M. Caricato, X. Li, H. P. Hratchian, A. F. Izmaylov, J. Bloino, G. Zheng, J. L. Sonnenberg, M. Hada, M. Ehara, K. Toyota, R. Fukuda, J. Hasegawa, M. Ishida, T. Nakajima, Y. Honda, O. Kitao, H. Nakai, T. Vreven, J. A. Montgomery Jr., J. E. Peralta, F. Ogliaro, M. Bearpark, J. J. Heyd, E. Brothers, K. N. Kudin, V. N. Staroverov, R. Kobayashi, J. Normand, K. Raghavachari, A. Rendell, J. C. Burant, S. S. Iyengar, J. Tomasi, M. Cossi, N. Rega, N. J. Millam, M. Klene, J. E. Knox, J. B. Cross, V. Bakken, C. Adamo, J. Jaramillo, R. Gomperts, R. E. Stratmann, O. Yazyev, A. J. Austin, R. Cammi, C. Pomelli, J. W. Ochterski, R. L. Martin, K. Morokuma, V. G. Zakrzewski, G. A. Voth, P. Salvador, J. J. Dannenberg, S. Dapprich, A. D. Daniels, Ö. Farkas, J. B. Foresman, J. V. Ortiz, J. Cioslowski and D. J. Fox, Gaussian, Inc., Wallingford, CT, 2009.
22. W. H. Koppenol and J. D. Rush, *J. Phys. Chem.*, 1987, **91**, 4429.
23. X. Nie, M. R. Esopi, M. J. Janik and A. Asthagiri, *Angew. Chem., Int. Ed.*, 2013, **52**, 2459.
24. X. Nie, W. Luo, M. J. Janik and A. Asthagiri, *J. Catal.*, 2014, **312**, 108.
25. J. P. Perdew, K. Burke and M. Ernzerhof, *Phys. Rev. Lett.*, 1996, **77**, 3865.
26. S. Grimme, J. Antony, S. Ehrlich and H. Krieg, *J. Chem. Phys.*, 2010, **132**, 154104.
27. S. Grimme, S. Ehrlich and L. Goerigk, *J. Comput. Chem.*, 2011, **32**, 1456.
28. G. Kresse and J. Hafner, *Phys. Rev. B*, 1993, **47**, 558.
29. G. Kresse and J. Hafner, *Phys. Rev. B*, 1994, **49**, 14251.
30. G. Kresse and J. Furthmüller, *Phys. Rev. B*, 1996, **54**, 11169.

31. G. Kresse and J. Furthmüller, *Comput. Mater. Sci.*, 1996, **6**, 15.
32. VASP Manual, https://www.vasp.at.
33. P. E. Blöchl, *Phys. Rev. B*, 1994, **50**, 17953.
34. G. Kresse and D. Joubert, *Phys. Rev. B*, 1999, **59**, 1758.
35. J. Heyd, G. E. Scuseria and M. Ernzerhof, *J. Chem. Phys.*, 2003, **118**, 8207.
36. J. Heyd and G. E. Scuseria, *J. Chem. Phys.*, 2004, **121**, 1187.
37. J. Heyd, G. E. Scuseria and M. Ernzerhof, *J. Chem. Phys.*, 2006, **124**, 219906.
38. G. Mills, H. Jónsson and G. K. Schenter, *Surf. Sci.*, 1995, **324**, 305.
39. A. A. Peterson, F. Abild-Pedersen, F. Studt, J. Rossmeisl and J. K. Nørskov, *Energy Environ. Sci.*, 2010, **3**, 1311.
40. S. N. Habisreutinger, L. Schmidt-Mende and J. K. Stolarczyk, *Angew. Chem., Int. Ed.*, 2013, **52**, 7372.
41. H. C. Hsu, I. Shown, H.-Y. Wei, Y.-C. Chang, H.-Y. Du, Y.-G. Lin, C.-A. Tseng, C.-H. Wang, L.-C. Chen, Y.-C. Lin and K.-H. Chen, *Nanoscale*, 2013, **5**, 262.
42. J. Graciani, K. Mudiyanselage, F. Xu, A. E. Baber, J. Evans, S. D. Senanayake, D. J. Stacchiola, P. Liu, J. Hrbek, J. F. Sanz and J. A. Rodriguez, *Science*, 2014, **345**, 546.
43. L. M. Azofra, D. R. MacFarlane and C. Sun, *Phys. Chem. Chem. Phys.*, 2016, **18**, 18507.
44. L. M. Azofra, D. R. MacFarlane and C. Sun, *Chem. Commun.*, 2016, **52**, 3548.
45. E. Skulason, G. S. Karlberg, J. Rossmeisl, T. Bligaard, J. Greeley, H. Jonsson and J. K. Nørskov, *Phys. Chem. Chem. Phys.*, 2007, **9**, 3241.
46. H. A. Hansen, J. Rossmeisl and J. K. Nørskov, *Phys. Chem. Chem. Phys.*, 2008, **10**, 3722.
47. N. Holmberg and K. Laasonen, *J. Phys. Chem. Lett.*, 2015, **6**, 3956.
48. J. Kibsgaard, C. Tsai, K. Chan, J. D. Benck, J. K. Nørskov, F. Abild-Pedersen and T. F. Jaramillo, *Energy Environ. Sci.*, 2015, **8**, 3022.
49. Q. Tang and D.-E. Jiang, *ACS Catal.*, 2016, **6**, 4953.
50. G. Gao, A. P. O'Mullane and A. Du, *ACS Catal.*, 2017, **7**, 494.
51. M. G. Mavros, T. Tsuchimochi, T. Kowalczyk, A. McIsaac, L.-P. Wang and T. V. Voorhis, *Inorg. Chem.*, 2014, **53**, 6386.
52. Y. Zheng, Y. Jiao, Y. Zhu, L. H. Li, Y. Han, Y. Chen, A. Du, M. Jaroniec and S. Z. Qiao, *Nat. Commun.*, 2014, **5**, 3783.
53. S. Piccinin, A. Sartorel, G. Aquilanti, A. Goldoni, M. Bonchio and S. Fabris, *Proc. Natl. Acad. Sci. U. S. A.*, 2013, **110**, 4917.
54. C. Ma, S. Piccinin and S. Fabris, *ACS Catal.*, 2012, **2**, 1500.
55. H.-Z. Wu, L.-M. Liu and S.-J. Zhao, *Phys. Chem. Chem. Phys.*, 2014, **16**, 3299.
56. J. K. Nørskov, J. Rossmeisl, A. Logadottir, L. Lindqvist, J. R. Kitchin, T. Bligaard and H. Jónsson, *J. Phys. Chem. B*, 2004, **108**, 17886.
57. J. H. Montoya, C. Tsai, A. Vojvodic and J. K. Nørskov, *ChemSusChem*, 2015, **8**, 2180.
58. L. M. Azofra, N. Li, D. R. MacFarlane and C. Sun, *Energy Environ. Sci.*, 2016, **9**, 2545.